THE JOURNAL OF BIOLOGICAL CHEMISTRY VOL. 283, NO. 5, pp. 2835–2845, February 1, 2008

Structure and Function of Sedoheptulose-7-phosphate Isomerase, a Critical Enzyme for Lipopolysaccharide Biosynthesis and a Target for Antibiotic Adjuvants*[S]

Received for publication, July 26, 2007, and in revised form, November 30, 2007 Published, JBC Papers in Press, December 3, 2007, DOI 10.1074/jbc.M706163200

Patricia L. Taylor[‡], Kim M. Blakely[‡], Gladys P. de Leon[‡], John R. Walker[§¶], Fiona McArthur[‖], Elena Evdokimova[§], Kun Zhang[‡], Miguel A. Valvano[‖1], Gerard D. Wright[‡2], and Murray S. Junop[‡3]

From the [‡]Department of Biochemistry and Biomedical Sciences, DeGroote School of Medicine, McMaster University, Hamilton, Ontario L8N 3Z5, the [§]Ontario Center for Structural Proteomics, Best Institute, Toronto, Ontario M5G 1L6, the [¶]Structural Genomics Consortium, University of Toronto, Toronto, Ontario M5G 1L5, and the [‖]Infectious Diseases Research Group, Siebens Drake Research Institute, Department of Microbiology and Immunology, University of Western Ontario, London, Ontario N6A 5C1, Canada

The barrier imposed by lipopolysaccharide (LPS) in the outer membrane of Gram-negative bacteria presents a significant challenge in treatment of these organisms with otherwise effective hydrophobic antibiotics. The absence of L-*glycero*-D-*manno*-heptose in the LPS molecule is associated with a dramatically increased bacterial susceptibility to hydrophobic antibiotics and thus enzymes in the ADP-heptose biosynthesis pathway are of significant interest. GmhA catalyzes the isomerization of D-sedoheptulose 7-phosphate into D-*glycero*-D-*manno*-heptose 7-phosphate, the first committed step in the formation of ADP-heptose. Here we report structures of GmhA from *Escherichia coli* and *Pseudomonas aeruginosa* in apo, substrate, and product-bound forms, which together suggest that GmhA adopts two distinct conformations during isomerization through reorganization of quaternary structure. Biochemical characterization of GmhA mutants, combined with *in vivo* analysis of LPS biosynthesis and novobiocin susceptibility, identifies key catalytic residues. We postulate GmhA acts through an enediol-intermediate isomerase mechanism.

Lipopolysaccharide (LPS)[4] is an essential component of the outer membrane in Gram-negative bacteria (1). LPS not only functions as a protective barrier preventing cell entry of hydrophobic molecules, including bile salts, detergents, and lipophilic antibiotics, but also helps maintain the structural integrity of the outer membrane. Thus, LPS is vital for bacterial virulence and antibiotic sensitivity in pathogenic Gram-negative bacteria.

Gram-negative pathogens are increasingly becoming a serious clinical threat. Multidrug-resistant hospital-acquired infections caused by enteric bacteria such as *Escherichia coli* and *Klebsiella pneumoniae*, and by emerging pathogens of environmental origin such as *Acinetobacter baumannii* and *Pseudomonas aeruginosa*, are the next big problem facing the infectious disease community. Furthermore, Gram-negative pathogens of animal origin such as *E. coli* O157-H7 are ongoing threats to agriculture and water quality. New chemotherapeutic strategies against Gram-negative bacteria are therefore required. LPS biosynthesis represents a unique Gram-negative target for new antimicrobial intervention.

LPS comprises lipid A, a core oligosaccharide, and in some bacteria, an *O*-specific polysaccharide chain. The core oligosaccharide has an inner core region consisting of 3-deoxy-D-manno-oct-2-ulosonic acid (Kdo) and one or more heptose units, and an outer core, consisting of additional sugar residues (Fig. 1*A*) (reviewed in Refs. 1–4).

Lipid A and Kdo are highly conserved in Gram-negative bacteria and essential for cell viability. The biosynthesis of these molecules is therefore a target for traditional antibiotic discovery efforts. Indeed, small molecule inhibitors of lipid A biosynthesis have been reported to have anti-Gram-negative activity (5).

Most Gram-negatives also contain one or more L-*glycero*-D-*manno*-heptose molecules attached to the Kdo. Mutants in

* This work was supported in part by grants from the National Science and Engineering Research Council (to M. A. V.), Special Program Grant Initiative "In Memory of Michael O'Reilly" funded by the Canadian Cystic Fibrosis Foundation and the Cardiovascular and Respiratory Health Institute of the Canadian Institutes of Health Research (to M. A. V. and G. D. W.), Canadian Cystic Fibrosis Foundation studentship (to P. L. T.), and the Canadian Institutes of Health Research (to G. D. W., and M. S. J., respectively). Use of the Advanced Photon Source was supported by the U. S. Dept. of Energy, Office of Science, Office of Basic Energy Sciences, under Contract DE-AC02-06CH11357. The costs of publication of this article were defrayed in part by the payment of page charges. This article must therefore be hereby marked "*advertisement*" in accordance with 18 U.S.C. Section 1734 solely to indicate this fact.

[S] The on-line version of this article (available at http://www.jbc.org) contains supplemental Figs. S1–S4, Tables S1 and S2, and a movie.

The atomic coordinates and structure factors (code 212W and 3BJZ) have been deposited in the Protein Data Bank, Research Collaboratory for Structural Bioinformatics, Rutgers University, New Brunswick, NJ (http://www.rcsb.org/).

[1] Holds a Canada Research Chair in Infectious Diseases and Microbial Pathogenesis.

[2] Holds a Canada Research Chair in Molecular Studies of Antibiotics.

[3] To whom correspondence should be addressed: 1200 Main St. West, Dept. of Biochemistry and Biomedical Sciences, 1200 Main St. West, Health Sciences Center, Rm. 4N20A, Hamilton, Ontario L8N 3Z5, Canada. Tel.: 905-525-9140 (ext. 22912); Fax: 905-522-9033; E-mail: junopm@mcmaster.ca.

[4] The abbreviations used are: LPS, lipopolysaccharide; DTT, dithiothreitol; Gln6P, glucosamine 6-phosphate; GmhA, sedoheptulose-7-phosphate isomerase; GmhB, D-heptose-1,7-bisphosphate phosphatase; HldE, bifunctional D-β-D-heptose phosphate kinase/D-β-D-heptose 1-phosphate adenyltransferase; Kdo, 3-deoxy-D-*manno*-oct-2-ulosonic acid; MIC, minimal inhibitory concentration; OM, outer membrane; PEG, polyethylene; S7P, D-sedoheptulose 7-phosphate; SeMet, selenomethionine; Tricine, *N*-[2-hydroxy-1,1-bis(hydroxymethyl)ethyl]glycine; r.m.s.d., root mean square deviation; Bis-Tris, 2-[bis(2-hydroxyethyl)amino]-2-(hydroxymethyl)propane-1,3-diol.

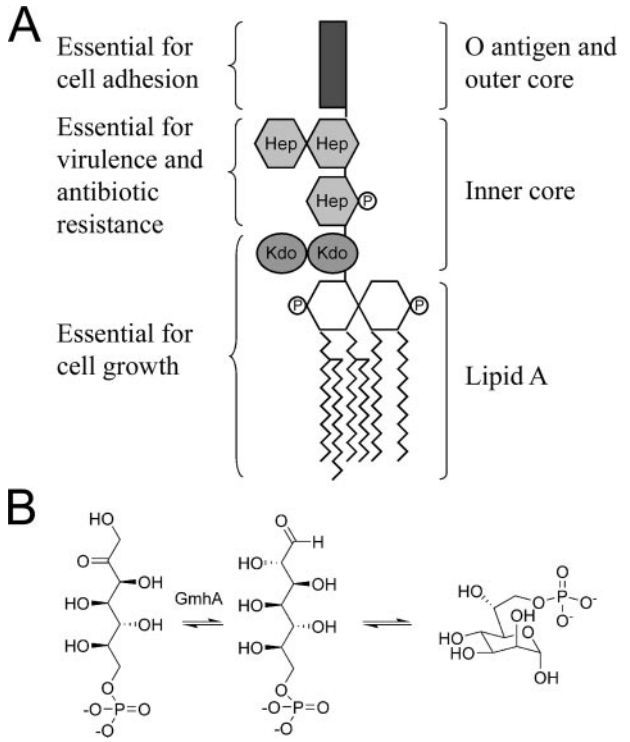

FIGURE 1. **LPS structure and activity of GmhA.** *A*, general structure of LPS in Gram-negative bacteria. *Kdo*, 3-deoxy-D-*manno*-oct-2-ulosonic acid; *Hep*, heptose; *P*, phosphate. *B*, schematic of the isomerase reaction catalyzed by GmhA, where D-sedoheptulose 7-phosphate is converted into D-*glycero*-D-*manno*-heptose 7-phosphate.

heptose metabolism, which are viable in laboratory conditions, are avirulent and highly susceptible to antibiotics (reviewed in Ref. 6). Heptose biosynthesis is thus a non-traditional target for Gram-negative selective antimicrobial agents. Inhibitors of heptose biosynthesis could be used as anti-virulence drugs or could be co-administered with antibiotics that do not normally cross the outer membrane barrier (*e.g.* novobiocin and erythromycin) to sensitize bacteria to these agents. We have termed such molecules antibiotic adjuvants (7).

The outer core carbohydrates and the *O*-specific polysaccharide side chains, also known as *O*-antigens, comprise the remainder of the LPS polymer. These components vary significantly by organism (1). They are not essential for cell growth but do mediate host-microbe interactions and play a significant role in virulence. Inhibitors of outer core and *O*-antigen biosynthesis could, therefore, be strategically deployed as organism-specific anti-virulence compounds.

All levels of LPS biosynthesis represent underexploited targets for new anti-microbial agents. The heptose biosynthetic pathway in Gram-negative bacteria, in particular, is highly attractive being essential for virulence and antibiotic sensitivity. Heptoses targeted to the inner core LPS are synthesized within the cytosol as ADP-activated L-*glycero*-β-D-*manno*-heptose molecules (8–10). Biosynthesis is initiated from D-sedoheptulose 7-phosphate (S7P). Sedoheptulose-7-phosphate isomerase (GmhA) catalyzes the first committed step in the pathway (Fig. 1*B*) (11–13). In *E. coli*, phosphorylation at the 1 position of the resulting in D-*glycero*-α,β-D-*manno*-heptose 7-phosphate is then catalyzed by the kinase moiety of the bifunctional D-β-D-heptosephosphate kinase/D-β-D-heptose-1-phosphate adenyltransferase (HldE) (14). A bifunctional HldE is also predicted in the opportunistic pathogen *P. aeruginosa* based on genomic sequence comparisons. However, in other pathogenic organisms, such as *Burkholderia cenocepacia*, this bifunctional enzyme is replaced by two distinct enzymes, HldA and HldC, which accomplish the respective functions (6, 15). D-α,β-D-Heptose-1,7-bisphosphate phosphatase (GmhB) catalyzes the removal of the phosphate at the 7 position, whereas the adenyltransferase action of HldE (or mono-functional HldC) transfers the AMP moiety from ATP to give ADP-D-*glycero*-β-D-*manno*-heptose (6, 16). Finally, ADP-D-β-D heptose epimerase (HldD) catalyzes the formation of ADP-L-*glycero*-β-D-*manno*-heptose, the precursor for the incorporation of heptose into the inner core, which is mediated by specific heptosyltransferases (17, 18).

A key step in ADP-heptose biosynthesis is S7P isomerization catalyzed by GmhA. Previous studies of GmhA predicted its function using gene deletion and product analysis (12, 13). Mutation of *gmhA* also results in a compromised OM, effectively removing the protective barrier normally afforded by LPS, therefore greatly increasing susceptibility to antibiotics (11). Understanding the structure and function of GmhA could aid in the future development of inhibitors that would increase the permeability of Gram-negative pathogens and act synergistically with known antibiotics as a novel treatment for Gram-negative infections.

We report crystal structures of *E. coli* and *P. aeruginosa* GmhA in apo, substrate, and product-bound forms and the use of this structural data to guide site-directed mutagenesis studies that enable prediction of the molecular mechanism of S7P isomerization, a potential target for new antimicrobial agents.

EXPERIMENTAL PROCEDURES

Purification of GmhA—Purification of *E. coli* GmhA followed a previously described protocol (19). An additional purification step was performed for GmhA protein used in crystallization and analytical ultracentrifugation studies. For these studies, GmhA was applied to a Q-Sepharose column (Amersham Biosciences Bioscience) and eluted using a linear KCl gradient (GmhA buffer A: 20 mM HEPES, pH 8.0, 1 mM EDTA, 5 mM dithiothreitol (DTT); GmhA Buffer B: 20 mM HEPES, pH 8.0, 1 mM EDTA, 5 mM DTT, 500 mM KCl). Fractions containing only GmhA were pooled and dialyzed extensively against 20 mM HEPES pH 8.0 and 4 mM DTT.

P. aeruginosa GmhA was overexpressed in *E. coli* BL21-Gold (DE3) (Stratagene), harboring an extra plasmid encoding three rare tRNAs (AGG and AGA for Arg and ATA for Ile). Cells were grown in auto-inducible media (20) for 4–5 h at 37 °C and 12–15 h at 20 °C. Cells were sonicated in binding buffer (5 mM imidazole, 5% glycerol, 50 mM sodium HEPES, pH 7.5, 0.5 M NaCl), supplemented with 1 mM phenylmethylsulfonyl fluoride and benzamidine and 0.5% IGEPAL CA-630 (Sigma). Clarified lysate was passed in series through DE52 and nickel-nitrilotriacetic acid (Qiagen) columns. GmhA was dialyzed in 10 mM sodium HEPES, pH 7.5, 0.5 M NaCl, and concentrated using a BioMax concentrator (Millipore). Selenomethionine (SeMet)-enriched protein was produced according to a previously

described procedure (21, 22). Tris(2-carboxyethyl)phosphine (0.5 mM) was added to all purification buffers.

Structure Determination of GmhA—All GmhA crystals were grown at 20 °C using the hanging drop/vapor diffusion method. *E. coli* GmhA (10 mg/ml) was mixed with an equal volume of crystallization solution (3% (w/v) polyethylene glycol (PEG)-8000, 0.1 M imidazole, pH 7.3, and 3% (v/v) ethylene glycol) and dehydrated against 1.5 M $(NH_4)_2SO_4$. For crystallization of substrate bound GmhA, S7P (see below) was added at a final concentration of 1 mM, and ethylene glycol was replaced with 1,6-hexandiol. Prior to flash freezing in liquid nitrogen, apo- and substrate-bound GmhA crystals were soaked (~30–60 s) in a cryo-protecting solution (10 mM HEPES, pH 7.3, 2 mM DTT, 1.5% PEG-8000, 50 mM imidazole, 3% ethylene glycol, 30% glycerol; or 0.5 mM S7P, 15.45 mM HEPES, pH 7.3, 3.1 mM DTT, 2.31% PEG-8000, 77.27 mM imidazole, 4.67% 1,6-hexandiol, 30% glycerol, respectively). *P. aeruginosa* apo-GmhA SeMet crystals grew in a solution of 25% PEG-3350, 0.1 M ammonium sulfate, and 0.1 M Bis-Tris, pH 5.5, and were cryoprotected with a mixture of 8% glycerol, 8% ethylene glycol, and 8% sucrose. Product-bound GmhA crystallized in a solution of 2.5 mM S7P (Sigma), 2 M ammonium sulfate, 0.2 M potassium/sodium tartrate and 0.1 M sodium citrate, pH 5.6, and were cryoprotected with 25% ethylene glycol. All x-ray diffraction data sets were collected at 100 K. *E. coli* apo and substrate-bound GmhA data were collected with an R-AXIS IV image-plate detector mounted on an RU300 rotating-anode x-ray generator (Rigaku/MSC Ltd.). Data sets were processed and scaled using d*TREK (23). An initial search model for molecular replacement using MOLREP (24) was generated from *V. cholerae* GmhA (25), PDB code 1X94. Substrate-bound GmhA was solved by molecular replacement using the refined *E. coli* apo-GmhA structure as a search model. *P. aeruginosa* SeMet GmhA single wavelength anomolous diffraction data were collected at the 19ID beamline of the Structural Biology Center, Advanced Photon Source, Argonne National Laboratory, whereas product-bound GmhA data were collected at the 17ID beamline of the Industrial Macromolecular Crystallography Association Collaborative Access Team. These data were processed with HKL2000 (26). Using SOLVE (27), all 20 expected selenium sites in the asymmetric unit were located. Resolve (28) was then used to build an initial model. To determine the structure of product-bound *P. aeruginosa* GmhA, the structure of the SeMet *P. aeruginosa* GmhA was used as a search model. Model building and refinement for all GmhA structures were carried out using O (29), Coot (30), REFMAC5 (31), or CNS (32), until *R* values and model geometry statistics fell within acceptable ranges (Table 1, under "Results"). Surface area calculations were performed using POPSCOMP (33). Structural illustrations were generated using PyMOL Molecular Graphics System (DeLano Scientific).

GmhA Mutagenesis—Site mutations in *E. coli gmhA* were generated in both pET28a(+)*gmhA* and pBAD30*gmhA* inserts using the QuikChange site-directed mutagenesis protocol (Stratagene). Sequences of mutagenic oligonucleotide primers are described in supplemental Table S1. Mutations were verified by DNA sequence analysis (MOBIX, McMaster University) using vector-specific sequencing primers (supplemental Table S1).

Sedimentation Equilibrium—*E. coli* GmhA and GmhA-D94N molecular weights in solution were determined by sedimentation equilibrium analysis using a Beckman-Coulter XL-1 analytical ultracentrifuge (Palo Alto, CA). Protein concentrations corresponding to 0.1, 0.2, and 0.4 $A_{280\ nm}$ values, respectively, were loaded into a six-channel epon-charcoal cell with a 1.2-cm path length. Equilibrium was allowed to develop for 12–14 h at rotor speeds of 20,000 and 25,000 rpm. The reference solvent contained 20 mM HEPES, pH 8.0, 150 mM KCl, 5 mM DTT (ρ = 1.006 g/ml). Absorbance data were collected at 280 nm and analyzed using the Beckman-Coulter Optima XL-1 Analytical Ultracentrifuge Origin Data Analysis Package (version 60-4) and Microcoal Origin 6.0. GmhA partial specific volume (0.739 ml/g), and solvent densities were determined using SEDNTERP, a public domain program developed by Hayes, Laue, and Philo. Resulting gradients were then fit to a self-association model using the above software. Due to the poor absorption of GmhA, high protein concentrations were required for detection, prohibiting accurate K_d determination.

Sedoheptulose 7-Phosphate Synthesis—S7P was synthesized enzymatically from D-serine and ribose 5-phosphate based on the protocol by Lee and colleagues, with minor modifications (34). *E. coli* transketolase was purified as previously described (19). Porcine D-amino acid oxidase (gift of V. Massey) was purified from *E. coli* BL21(DE3)/pET28a(+)DAO cells by anion exchange using a Q-Sepharose column. Purified protein was analyzed using 12% SDS-PAGE, and activity was confirmed using a lactate dehydrogenase-coupled enzyme assay (35). D-amino acid oxidase was stored in the presence of 5 mM FAD. S7P synthesis and purity was determined using liquid chromatography/electrospray mass spectrometry and ^{1}H, ^{13}C, and ^{31}P NMR.

E. coli GmhA Steady-state Kinetic Analysis—GmhA activity was monitored by coupling product formation to HldE and GmhB and monitoring P_i release, as previously described (19) with the following modifications. The reaction mixture consisted of 20 mM HEPES, pH 8.0, 10 mM MgCl, 10 mM KCl, 6 mM ATP, 0.4% Tween 20, 0.214 nmol of GmhA, 0.375 nmol of GmhB, 0.094 nmol of HldE, and 0.2 unit of pyrophosphatase in a total volume of 90 μl. Reactions were initiated with 10 μl of S7P for final concentrations ranging from 0 to 2 mM. Initial rates were fit to Equation 1 describing Michaelis-Menten kinetics using Grafit 4 software (Erithacus Software, Staines, UK).

$$v = k_{cat}E_t[S]/(K_m + [S]) \quad \text{(Eq. 1)}$$

GmhA in Vivo Complementation Studies—pBAD30*gmhA* wild-type and mutant vectors were used to transform *E. coli* BW25113Δ*gmhA* cells (36) to create complement strains. Positive and negative control strains were created by transforming the pBAD30 vector into *E. coli* BW25113 and *E. coli* BW25113Δ*gmhA* cells, respectively. Cells were cultured overnight at 37 °C, 250 rpm in M9 minimal media, 0.2% arabinose, 100 μg/ml ampicillin. To confirm GmhA expression, 1 ml of overnight culture was harvested, resuspended in 50 μl of 10 mM Tris, pH 7.5, 1 mM EDTA buffer, 50 μl of 2× SDS loading dye. Cells were lysed by boiling 30 min and analyzed by 15% SDS-PAGE. For immunoblot analysis, gel contents were transferred

TABLE 1
GmhA data collection and model refinement statistics

	Data set			
	Apo_{EC}	$Sub\text{-}bound_{EC}$	Apo_{PA}	$Product\text{-}bound_{PA}$
Data collection				
Space group	$P2_12_12_1$	$P2_1$	$P2_12_12$	$P6_522$
Cell parameters				
a,b,c (Å)	83.9, 89.6, 106.9	73.0, 76.5, 78.3	123.8, 131.6, 48.8	126.3, 126.3, 113.2
α, β, γ (°)	90, 90, 90	90, 106.1, 90	90, 90, 90	90, 90, 120
Molecules in ASU	4	4	4	2
Resolution (Å)[a]	45.93-1.95 (2.02-1.95)	47.39-2.79 (2.89-2.79)	40.0-2.40 (2.46-2.40)	40.0-2.30 (2.38-2.30)
Unique reflections	59,294	20,533	30,927	24,669
Redundancy[a]	4.27 (4.18)	2.63 (2.68)	7.6 (6.8)	12.4 (12.6)
Completeness (%)[a]	99.8 (100.0)	98.6 (99.4)	99.9 (100.0)	99.9 (100.0)
$I/\sigma(I)$[a]	10.9 (3.4)	6.7 (2.6)	29.1 (4.2)	25.0 (6.2)
R_{merge} (%)[a]	7.5 (39.8)	11.1 (36.0)	7.0 (40.0)	12.5 (40.4)
Model and refinement				
Resolution (Å)[a]	45.93-1.95	25.0-2.80	39.19-2.40	39.3-2.30
R_{work} (%)	19.2	20.3	19.7	17.6
R_{free} (%)	22.4	25.7	27.4	22.1
$Reflections_{(observed)}$	56,213	18,807	29,349	24,221
$Reflections_{(Rfree)}$	2,996	1,478	1,578	1,222
No. residues/atoms	737/5,630	707/5,436	715/5,535	391/2,969
No. of waters	634	226	148	178
r.m.s.d. bond				
Lengths (Å)	0.013	0.024	0.010	0.019
Angles (°)	1.27	2.05	1.28	1.80
Mean *B* factor ($Å^2$)	36.7	45.6	35.1	29.1
PDB ID code	2I2W	2I22	3BJZ	1X92

[a] Statistics for the highest resolution shell are shown in parentheses.

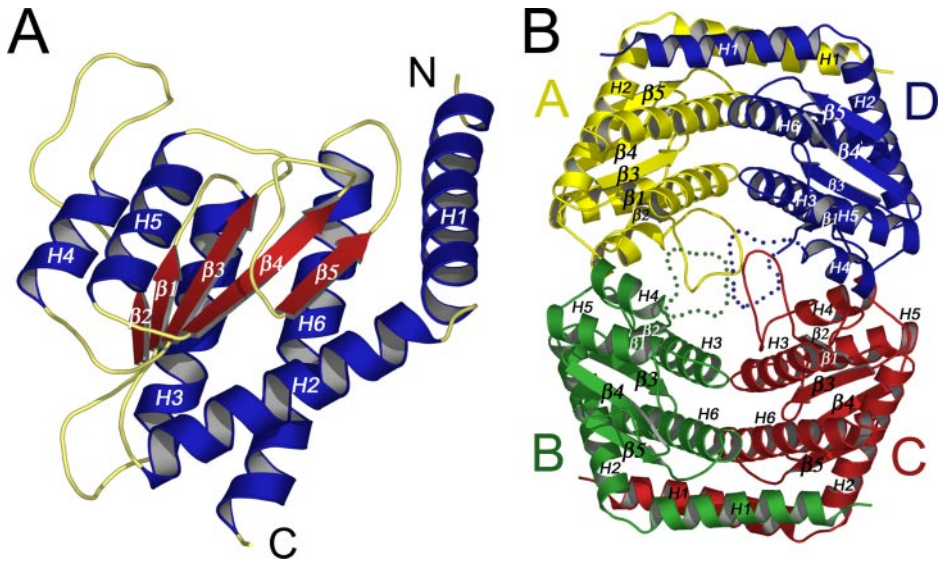

FIGURE 2. **Structure of the *E. coli* GmhA apoprotein.** *A*, GmhA monomer. β-Strand and α-helix in *red* and *blue*, respectively; *B*, GmhA tetramer. *Dashed lines* in subunits B and D represent disordered regions of GmhA not observed in the final model.

to a polyvinylidene fluoride membrane. GmhA was detected using mouse IgG anti-histidine primary antibody (Amersham Biosciences) and peroxidase-conjugated Affini-pure donkey anti-mouse IgG secondary antibody (Jackson Immuno-Research). PerkinElmer Life Sciences Western lighting chemiluminescence reagent was used in detection. Minimal inhibitory concentrations (MIC) of novobiocin were determined as follows: Overnight cultures, as described above, were diluted to $A_{600\ nm}$ 0.11 and further diluted 1 in 200. Strains were grown at 37 °C in 96-well plates in the presence of varying concentrations of Me_2SO-dissolved novobiocin (2–1024 μg/ml). $A_{600\ nm}$ was measured after 20 h to assay growth. MIC was determined as the concentration of novobiocin required to reduce the $A_{600\ nm}$ of each strain to 90% of the $A_{600\ nm}$ in the absence of drug.

LPS Analysis—E. coli BW25113 Δ*gmhA*/pBAD30*gmhA* wild-type and mutant strains were grown at 37 °C for 24 h on M9 minimal media, 0.2% arabinose, 100 μg/ml ampicillin agar plates. LPS was extracted from these cells as previously described (37). LPS samples were analyzed by 10% SDS-PAGE in the Tricine buffer system and detected by silver staining (37, 38). Gels were fixed overnight in 250 ml of fixing solution (60% MeOH, 10% acetic acid). Gels were washed, in order, using 200 ml of 7.5% acetic acid for 30 min, 200 ml of 0.7% periodic acid for 30 min, milliQ H_2O for 3 × 15 min, 200 ml of staining solution (42 ml of 0.36% NaOH, 2.8-ml concentrated NH_4OH, 8 ml of 19.4% silver nitrate, 148 ml of H_2O) for 25 min, milliQ H_2O for 2 × 15 min, and 200 ml of developing solution (50 mg of citric acid, 0.5 ml of 37% formaldehyde in H_2O) until bands appear. Stain development was stopped by repeated washing in H_2O.

RESULTS

Structural Analysis of GmhA—The crystal structures of apo-GmhA from *E. coli* and *P. aeruginosa* were determined to 1.95 Å (PDB 2I2W) and 2.4 Å (PDB 3BJZ), respectively (Table 1). The structure from *E. coli* was solved via molecular replacement using an initial model based on the GmhA structure from *V. cholerae* (PDB 1X94). *E. coli* apo-GmhA crystals grew in the

space group $P2_12_12_1$ with four molecules of GmhA in each asymmetric unit as shown in Fig. 2 (subunits A, B, C, and D). Analysis of oligomerization using the program PISA (39) strongly suggested that GmhA would exist in solution as a tetramer. This was further verified by sedimentation equilibrium studies (supplemental Fig. S1). No electron density was observed for residues 83–97 in chains B or D, and therefore these regions are represented as *dotted lines* in Fig. 2. Three intersubunit Cys–Cys disulfide linkages were observed in the asymmetric unit, one at Cys-90 linking chain A–C, and two others linking Chains A–B and C–D at Cys-57, respectively. These linkages are likely artifacts, because addition of a reducing agent or substitution of Cys to Ser resulted in increased GmhA activity (discussed below). The A–D and B–C dimer interfaces are extensive (2680 Å^2), each resulting from reciprocal interactions between helices H1, H3, and H6. A–B and C–D interfaces are less extensive (1515 Å^2) and are formed primarily through H4 and reciprocal interactions with loop regions joining H3–β2 or β2–H4. The final model was refined to R and R_{free} values of 19.2 and 22.4, respectively. Apo-GmhA from *P. aeruginosa* was crystallized in space group $P2_12_12$, and the structure was determined to 2.4 Å using SeMet-substituted protein and single-wavelength anomalous diffraction. The final model was refined to R and R_{free} values of 19.7 and 27.4, respectively. As with the apo-GmhA structure from *E. coli*, a tetramer of GmhA was observed in the asymmetric unit and residues 83–96 in each chain were disordered. The Cα traces of these monomers could be superimposed with an r.m.s.d. of 1.1 Å (supplemental Fig. S2).

Each GmhA monomer consists of a central five-stranded parallel β-sheet, flanked by five alpha helices (Fig. 2*A*), forming a three-layered HβH sandwich. Helical layers are composed of H2, H3, and H6 on one side and H4 and H5 on the opposing side of the central β-sheet with topology β2, 1, 3, 4, and 5. The overall fold is quite similar to the flavodoxin-type nucleotide-binding motif and is essentially identical to GmhA structures from *V. cholerae* (PDB 1X94) and *Campylobacter jejuni* (PDB 1TK9) (25).

In addition to apo-structures of GmhA, we also determined structures of GmhA in the presence of substrate and product. The structure of *E. coli* GmhA in complex with S7P was determined to 2.79 Å (PDB 2I22). This complex crystallized in a different space group ($P2_1$) compared with apoprotein. The final model was refined to R and R_{free} values of 20.3 and 25.7, respectively. The major difference observed between the apoprotein and substrate-bound complex, aside from the presence of S7P, centers on the loop connecting β2 and H4, which becomes disordered in the presence of substrate (Fig. 3*A*). Because wild-type GmhA isomerase was used to generate these crystals, and crystals took several days to grow, a mixture of product and substrate is expected to have been present during crystal formation. Clear additional electron density was observed at only one of the four potential active sites within the GmhA tetramer. As shown in Fig. 4*A*, this density is consistent with the presence of substrate; however, given the relatively low resolution to which this structure was determined, further structural and functional analysis was required to fully characterize the active site of GmhA.

The product-bound structure of GmhA from *P. aeruginosa* was determined in space group $P6_522$ to 2.3 Å (PDB 1X92). These crystals were generated following incubation of GmhA with substrate (see "Experimental Procedures"). In this case, clear electron density corresponding to product was observed in each active site region (Fig. 4*B*). In contrast to the apo and substrate-bound structures of *E. coli* GmhA, the product-bound protein crystallized as a dimer in the asymmetric unit (Fig. 3*A*). However, by combining two dimers from crystallographic related symmetry mates, a tetramer could be generated (Fig. 3*B*).

Because wild-type GmhA was used in all of these studies, it would appear that crystallization conditions (as opposed to an inactive GmhA) were responsible for selecting distinct conformations of GmhA capable of binding either substrate or product.

To date, six structures of GmhA have been determined: apo and substrate-bound *E. coli* GmhA, apo and product-bound *P. aeruginosa* GmhA, *V. cholera* GmhA, and *C. jejuni* GmhA. As shown in Fig. 5, these structures can be categorized into two distinct conformations, designated "open" and "closed." The *E. coli* structures as well as the apo *P. aeruginosa* and the *V. cholerae* structures adopt an open conformation, whereas the *P. aeruginosa* and *C. jejuni* exist in the closed state. Three major differences between the open and closed conformations are apparent. First, a new helix (H3′) in the product-bound structure is present in place of the disordered loop located between β2–H4 in the apo and substrate-bound structures (Fig. 3*A*, *purple arrow*). A second difference is the overall positioning of the loop joining H3 and β2. In the closed state this loop is rotated inward toward the opposing subunit by ~20 Å relative to the open conformation (Fig. 3*A*, *red arrow*), with the exception of apo *P. aeruginosa*, where the H3–β2 loop is in line with the closed conformation rather than the open. Finally, compared with the open conformation structures, the tetramer formed in the closed conformation structures is more compact and bury substantially more dimer-dimer surface area (2500 *versus* 1250 Å^2) due to the packing of H3′. Fig. 3 (*B* and *C*) illustrates the difference between these two tetrameric forms, highlighting a large reorganization of the dimer-dimer interface. Bringing dimers of product-bound GmhA together involves a corkscrew-like movement with concerted translational (5 Å) and rotational (25°) movements between A–D and B–C dimers (see the supplemental movie illustrating the structural transition between open and closed conformations, as illustrated in Fig. 3*B*). As shown in Fig. 3*D*, the formation of H3′ in the closed conformation of GmhA is responsible for repositioning the H3–β2 loop due to steric hindrance.

Both substrate and product are found at the interface formed between subunits A and D. As discussed above, only one of the four active sites within GmhA contained substrate, whereas the structure of product-bound GmhA contained fully occupied active sites. In the S7P-bound structure numerous contacts were observed between substrate and the following amino acid

side chains (supplemental Table S2): Ser-55, Thr-120, Asp-169, and Gln-172 of chain D, and His-61, Glu-65, and His-180 of chain A. In general, the active sites observed for both the substrate and product-bound structures are comparable (Fig. 4). Several residues from both structures remain unchanged, in particular: Ser-55 (Ser-54), Ser-119, Thr-120, Ser-121, Ser-124, and His-180 (His-182) (residues in parentheses correspond to product-bound *P. aeruginosa* GmhA). Although not perfectly superimposible, side chains from residues Glu-65 (Glu-64) and Gln-172 (Gln-174) did not differ significantly in their overall position between the two structures. In contrast, residues His-61 (His-60) and Arg-69 (Arg-68) adopt different positions largely due to the dramatic change of position in the H3–β2 loop. The most striking difference, however, occurs in the product-bound form, by additional contacts made with residues Asn-93 and Asp-94 of chain B (Fig. 4*B*). The finding that residues from three chains (A, B, and D) are involved in binding product suggests that assembly of a GmhA tetramer may be required for function.

Rationale for Site-directed Mutagenesis—Potential GmhA active site residues were chosen for analysis based on crystallographic active site data of both the substrate-bound *E. coli* enzyme and product-bound *P. aeruginosa* enzyme (Fig. 4). A total of eight residues was selected for analysis and is described by *E. coli* residue number. Equivalent residues of Glu-65, Thr-120, and Gln-172 show direct contact in both substrate and product bound crystal structures. The highly conserved Ser-55, Ser-119, Thr-120, Ser-121, and Ser-124 pocket was hypothesized to bind the S7P phosphate, rather than play a direct role in catalysis. As such, only one residue from this pocket, Thr-120, was chosen for mutagenesis. His-61, Asp-169, and His-180 contacts are unique to the *E. coli* substrate-bound structure, whereas Arg-69 and

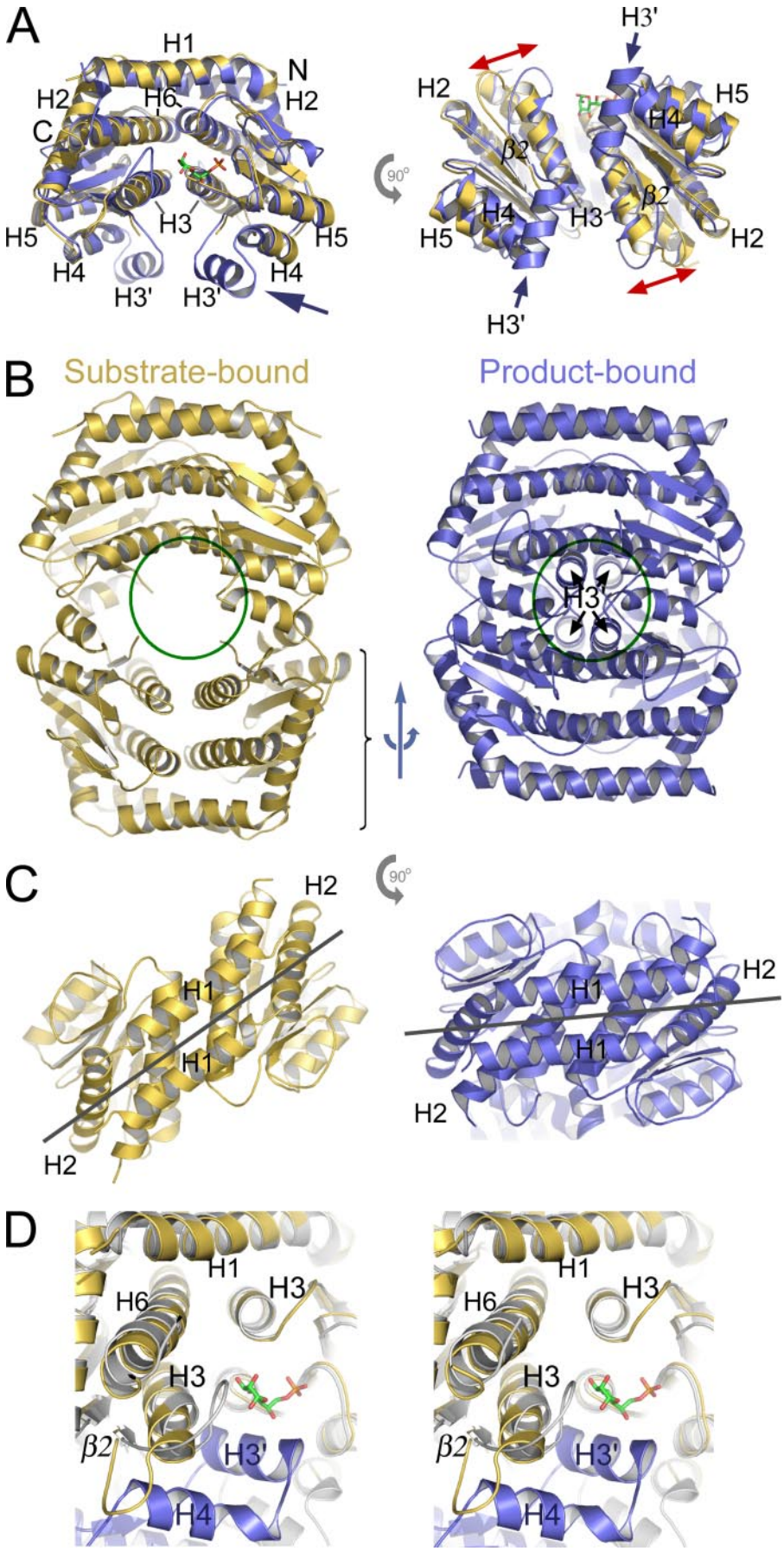

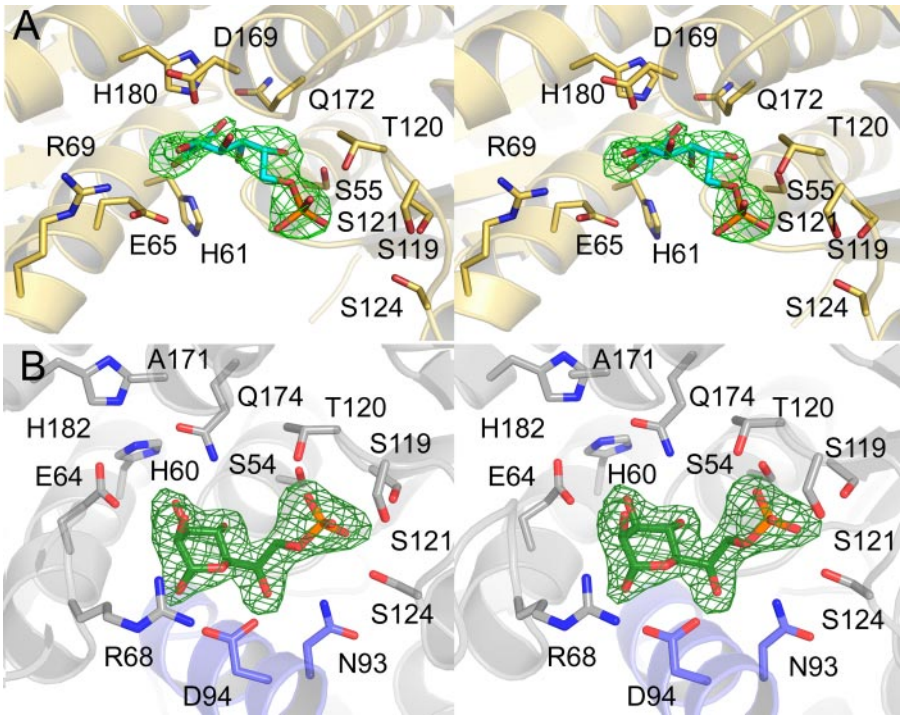

FIGURE 4. **Stereo view of active site structures of substrate and product-bound GmhA.** *A*, *E. coli* GmhA in complex with S7P; *B*, *P. aeruginosa* GmhA in complex with D-*glycero*-D-*manno*-heptose 7-phosphate. All amino acid side chains making direct interaction with either substrate (*A*) or product (*B*) are shown. Product and substrate $F_o - F_c$ omit maps ($\sigma = 3.0$) are presented.

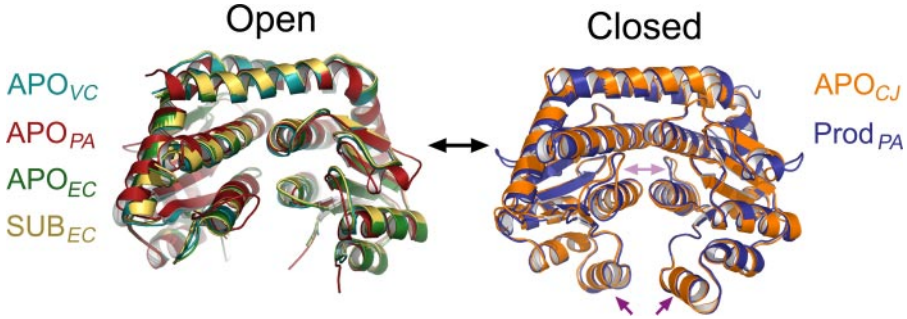

FIGURE 5. **Structural comparison of all known GmhA structures.** Aligned structures were grouped into either the open or closed conformation. *Light* and *dark purple arrows* highlight structural transitions involving the H3–β2 loop and H3′ helix, respectively.

Asp-94 contacts are unique to the *P. aeruginosa* product-bound structure. As shown in Fig. 6, all mutated residues are conserved across Gram-negative species, with the exception of Asp-169. Asp-169 was examined even without conservation due to its prominent position depicted in the *E. coli* active site.

In Vitro Mutational Analysis—The ability of purified *E. coli* GmhA wild-type and mutant proteins to convert enzymatically synthesized S7P into product was assessed using a coupled assay monitoring P_i release. Initial studies, using wild-type GmhA, determined that synthesized S7P was indeed a substrate of GmhA, and that the reaction was linear for at least 10 min in the presence of 0.214 nmol of protein. Purified mutant GmhA proteins were then assayed for activity against S7P (Table 2). Of the eight mutants tested, only H61Q and R69Q demonstrated measurable *in vitro* activity. R69Q turnover ($0.45 \pm 0.1\ s^{-1}$) was equal to that of wild-type GmhA ($0.44 \pm 0.07\ s^{-1}$), whereas the turnover of H61Q ($0.23 \pm 0.07\ s^{-1}$) was roughly half that of wild type. The remaining GmhA mutants, E65N/Q, D94N, T120A, D169N, Q172E, and H180Q, showed undetectable *in vitro* activity (limit of detection, $0.003\ s^{-1}$ at 2 mM S7P).

In Vivo Mutational Analysis—To further explore the role of each residue in the active site, *in vivo* complementation studies were performed using *E. coli* BW25113 Δ*gmhA*/pBAD30*gmhA* wild-type and mutant-expressing strains. A positive control strain, *E. coli* BW25113/pBAD30 (wild-type plus vector only), and negative control strain, *E. coli* BW25113Δ*gmhA*/pBAD30 (*gmhA* deletion plus vector only), were also generated. Equivalent amounts of GmhA expression, and therefore complementation to the chromosomal deletion, were confirmed in each mutant strain by anti-histidine immunoblot (supplemental Fig. S3).

The growth of each *gmhA*-expressing strain was analyzed to ensure the overexpression of *gmhA* did not have adverse effects. For the first 20 h, growth of all strains was consistent, as measured by $A_{600\ nm}$. After 20-h growth, the $A_{600\ nm}$ of E65N-, E65Q-, Q172E-, H180Q-, and D94N-expressing strains, as well as the negative control strain, reached a maximum of ~0.6, and actually began to decrease with time. Conversely, the remaining strains continued to increase in $A_{600\ nm}$ after 18 h growth. By 48 h, however, the $A_{600\ nm}$ of all strains reached a consistent

FIGURE 3. **Structural comparison of substrate and product-bound GmhA.** *E. coli* GmhA complexed with S7P (*gold*) and *P. aeruginosa* GmhA compexed with D-*glycero*-D-*manno*-heptose 7-phosphate (*blue*). *A*, two *orthogonal views* of the A–D dimer are presented. *Blue* and *red arrows* illustrate formation of new H3′ helix and repositioning of the H3–β2 loop, respectively. *B*, comparison of change in quaternary structure between substrate and product-bound GmhA tetrameric forms. The *green circle* highlights relative position of four H3′ helices formed in presence of product. The *blue arrows* illustrate the translational and rotational differences of the dimer-dimer interface between substrate and product-bound forms. See the supplemental movie illustrating conformational changes between substrate and product bound forms of GmhA. *C*, same illustration as presented in *B*, but from the *bottom* of the structure. *Light gray lines* illustrate the relative rotational difference between equivalent BC dimers of the substrate- and product-bound structures. *D*, close-up *stereo view* comparing the relative positions of H3 and H3–β2 loop regions of substrate and product-bound GmhA. *Blue*, subunit B of product-bound structure.

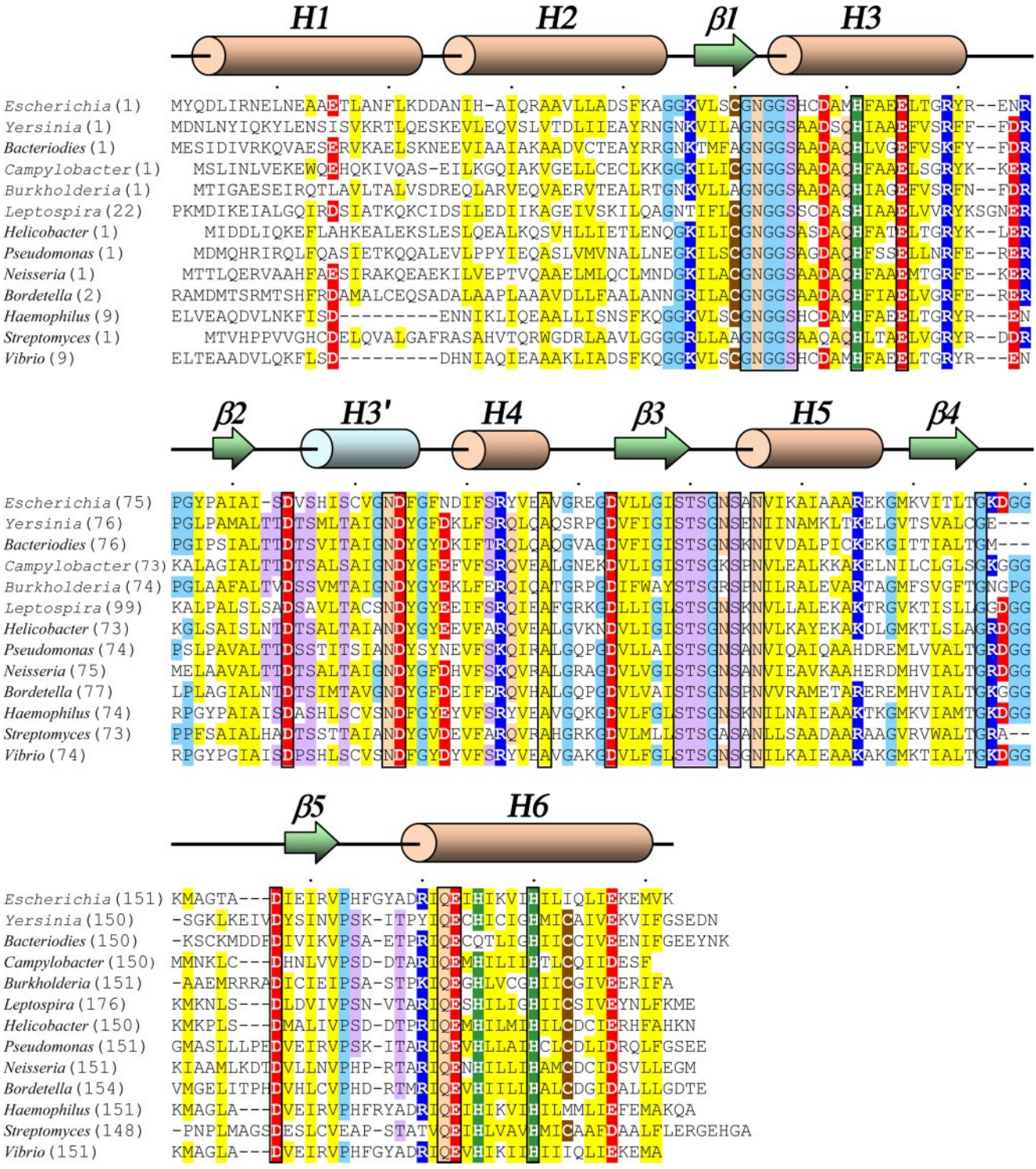

FIGURE 6. **Sequence alignment of GmhA from various bacterial pathogens.** *Boxed residues* are completely conserved between organisms. *Colors* indicate properties of conserved residues: *Yellow*, partial conservation; *red*, acidic; *dark blue*, basic; *pale blue*, Gly/Pro; *pink*, Asn/Gln; *green*, His; *brown*, Cys; and *purple*, Ser/Thr.

level, suggesting the presence or absence of GmhA, whether present in basal or overexpressed levels, has little effect on the growth of *E. coli* cells.

The susceptibility of these mutant *gmhA* complemented strains to the antibiotic novobiocin was then examined (Fig. 7*A*). Under normal wild-type conditions with an intact LPS, *E. coli* is insensitive to novobiocin. In contrast, *E. coli* exhibiting a deep-rough phenotype, where only lipid A and Kdo are synthesized, display increased sensitivity to novobiocin (40). This property was confirmed in the control strains, with the positive control exhibiting a novobiocin MIC of 1024 μg/ml, compared with an MIC of 64 μg/ml determined for the negative control (*gmhA* deletion, heptoseless) strain. The H61Q, R69Q, T120A, and D169N complement strains were able to completely

TABLE 2

Summary of kinetic parameters of wild type and mutant *E. coli* GmhA purified proteins

GmhA activity was determined using the malachite green phosphate detection assay by coupling product formation to HldE and GmhB and monitoring the release of inorganic phosphate spectrophotometrically at 660 nm. Reactions were initiated with S7P to final concentrations of 0–2 mM. A detection limit of 0.003 s^{-1} was determined for this assay.

GmhA mutant	k_{cat}	K_m	k_{cat}/K_m
	s^{-1}	mM	$mM^{-1}\ s^{-1}$
Wild type	0.44 ± 0.7	0.9 ± 0.3	0.5
H61Q	0.23 ± .07	1.2 ± 0.7	0.2
E65N	<0.003		
E65Q	<0.003		
R69Q	0.45 ± 0.1	0.5 ± 0.3	0.9
D94N	<0.003		
T120A	<0.003		
D169N	<0.003		
Q172E	<0.003		
H180Q	<0.003		

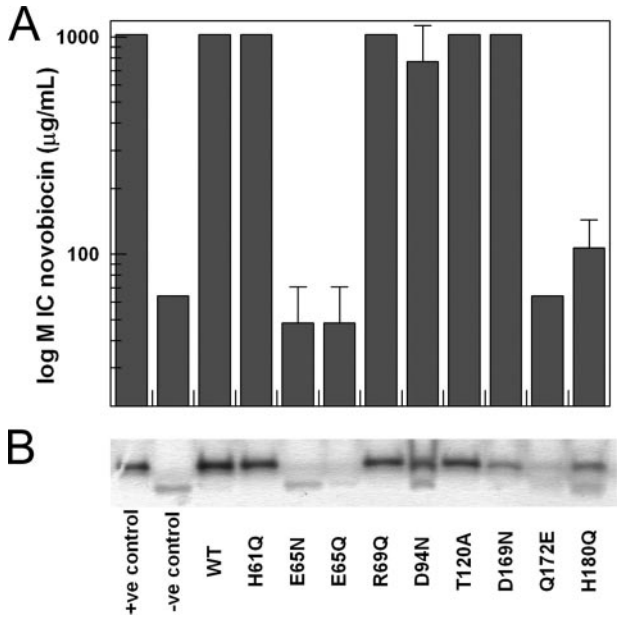

FIGURE 7. **Novobiocin MIC and LPS analysis of GmhA mutants.** *A*, minimum concentration of novobiocin required to inhibit the growth of *E. coli* BW25113pBAD30 (*+ve control*), BW25113Δ*gmhA* pBAD30 (*-ve control*), and BW25113Δ*gmhA* pBAD30*gmhA* mutant strains as described, to 90% of standard growth in the absence of drug (MIC). Strains were grown in M9 minimal media supplemented with 0.2% arabinose and 0–1024 μg/ml novobiocin. *B*, LPS analysis of *E. coli* BW25113Δ*gmhA* pBAD30*gmhA* mutants by silver-stained 10% SDS-PAGE. LPS was extracted from cultures of the above strains, grown overnight in M9 minimal media plus 0.2% arabinose.

restore novobiocin resistance to positive control levels (Fig. 7*A*). The D94N strain showed increased sensitivity to drug within one dilution. The Glu-65 mutant-expressing strains, as well as Q172E and H180Q mutational strains, exhibited reduced MIC values. MIC values in each case approximated within one drug dilution that of the negative control strain. The strain expressing H180Q demonstrated a slightly higher MIC value, whereas the strain expressing E65N/Q had slightly lower values. This represents a 10-fold decrease in MIC when compared with wild-type levels.

Intact LPS was extracted from each of the deleted *gmhA* strains containing the plasmids expressing the GmhA mutant forms and analyzed using silver stained 10% SDS-PAGE. When viewed in this manner, truncated LPS can be differentiated from full-length LPS based on relative migration distance, because truncated LPS migrates much faster through the gel. As depicted in Fig. 7*B*, H61Q, R69Q, T120A, and D169N GmhA replacements did not affect LPS production, because the *gmhA*-deleted strains containing these proteins produce full-length LPS. The remaining five GmhA constructs (E65N/Q, D94N, Q172E, and H180Q) resulted in at least partially truncated LPS. The complete truncation due to both Glu-65 mutant-expressing strains was consistent with MIC data, suggesting substantially reduced GmhA activity. Surprising, however, was the partial truncation due to Q172E and H180Q mutations. GmhA containing these mutations appear to be at least partially active *in vivo*. The partial truncation of D94N is also somewhat contradictory to MIC results, although the D94N-expressing strain demonstrated decreased novobiocin MIC compared with wild type. Based on these data, it appears that complete LPS truncation is not required to sensitize *E. coli* to novobiocin. Rather, LPS can be partially truncated, as observed in the D94N mutant without compromising the membrane to a threshold limit, beyond which the permeability barrier is breached, as with the Q172E and H180Q mutants.

DISCUSSION

Structural Analysis of GmhA—We have determined the three-dimensional structures of GmhA from *E. coli* and the opportunistic bacterial pathogen *P. aeruginosa*, in apo, substrate- and product-bound forms. These structures complement available structures from *C. jejuni* and *V. cholerae* that have recently emerged from structural genomics studies (25). The *E. coli* and *C. jejuni* proteins crystallize as tetramers in the asymmetric unit, whereas the *P. aeruginosa* and *V. cholerae* proteins crystallize as dimers; as is often the case, the contents of the crystallographic asymmetric unit do not necessarily reflect biological units of activity. Analytical ultracentrifugation studies performed in this work further suggest that the biologically active oligomeric state of GmhA is a tetramer. This interpretation is also supported by the extensive total surface areas buried in tetramer formation for apo (8400 $Å^2$), substrate (7550 $Å^2$), and product-bound (10380 $Å^2$) structures.

Of particular note when comparing the available structures of GmhA, is that all six available structures can be classified into either of two very distinct forms: an open and a closed form. The open form is characterized by an extended H3–β2 loop, an unstructured H3′ region, and a less well packed dimer-dimer interface. In the closed form the H3′ region adopts a helical structure that in turn causes not only repositioning of the H3–β2 loop inward toward the active site cleft by ~20 Å but also permits more extensive dimer-dimer interactions resulting in a more compact tetramer. The open conformation is observed in structures of GmhA in apo and substrate-bound forms from *E. coli* and also in the apo structures from *P. aeruginosa* and *V. cholera*. The closed conformation is observed in the apo and product-bound structures from *C. jejuni* and *P. aeruginosa*, respectively. The fact that only two conformations are observed despite structures having been determined in different space groups, from multiple organisms, and in three different states of ligand binding, suggests that GmhA is likely to exist in two distinct conformations. The open and closed conforma-

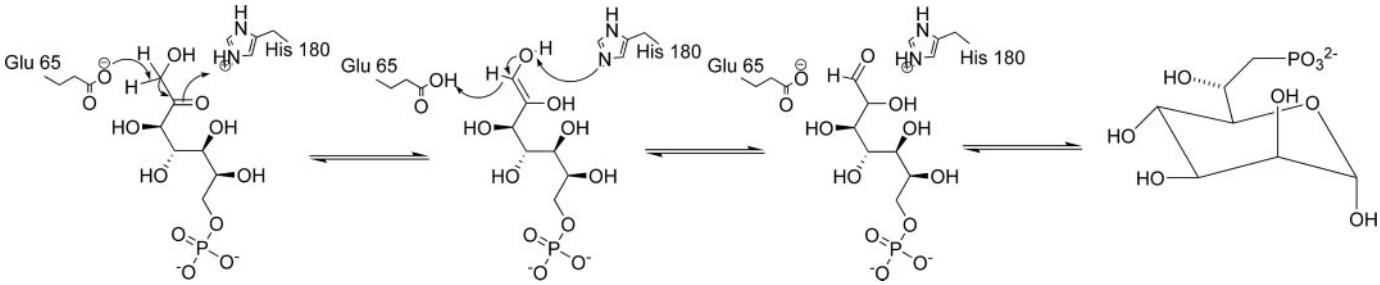

FIGURE 8. **Proposed mechanism of GmhA.** The GmhA catalyzed conversion of D-sedoheptulose 7-phosphate into D-*glycero*-D-*manno*-heptose 7-phosphate is predicted to proceed through an enediol intermediate, where Glu-65 serves as the catalytic base and His-180 serves as the catalytic acid.

tions represent structures most suited for binding substrate and product, respectively. GmhA is an isomerase and should be able to readily catalyze both forward and reverse reactions, suggesting that both S7P and D-*glycero*-α,β-D-*manno*-heptose 7-phosphate are "substrates" of GmhA. With this in mind, it is not surprising that the structure of *C. jejuni* GmhA crystallized in the product bound, closed conformation even with no ligand bound.

Determination of GmhA Mechanism of Action—Results from both *in vivo* and *in vitro* analysis of GmhA mutational studies suggest the importance of residues Glu-65, Gln-172, and His-180 in enzyme activity. Amino acid substitutions at Glu-65, Asp-94, Thr-120, Asp-169, Gln-172, and His-180 residues result in no observable GmhA activity when analyzed *in vitro* using the phosphate detection assay. Diminished activity of these mutants was expected, because these residues are all located within the active site. However, it was difficult to elucidate the actual role of these residues in GmhA action from kinetic analysis alone. For this reason, *in vivo* studies were performed. Both *in vitro* and *in vivo* studies suggest that His-61 and Arg-69 play no significant role in GmhA activity, because wild-type activity was maintained when each was mutated. Conversely, Glu-65, Gln-172, and His-180 were deemed necessary in maintaining the LPS permeability barrier as illustrated in novobiocin MIC studies and supported by LPS analysis, suggesting these residues are important to GmhA function. The remaining mutated residues, Asp-94, Thr-120, and Asp-169, did not alter the permeability of *E. coli* to novobiocin. This does not imply, however, that Asp-94, Thr-120, and Asp-169 have no role in activity. There are a number of reasons why these mutations show diminished activity *in vitro* and not *in vivo*, specifically the nature of each assay. Kinetic studies were designed to assay the reaction over a limited time period. Furthermore, mutant proteins were overexpressed *in vivo*, which could help to restore protein activity based on the quantity of protein in the cell. With this consideration in mind, overexpression can be advantageous in demonstrating inactivity, as even with an abundance of protein, the activity of Glu-65, Gln-172, and His-180 could not be completely, or in the case of Glu-65, even partially restored. The role of Thr-120 was hypothesized to be involved in substrate-phosphate binding, as previously predicted by analogy to glucose-6-phosphate isomerase (6). It is quite possible that the role of Thr-120 could be partially compensated by surrounding residues, in particular Ser-55, Ser-119, Ser-121, and Ser-124, which are also predicted to function in phosphate binding. The Asp-94 residue was not observed in the active site of the substrate-bound structure; rather, this mutation was designed based on contacts observed in the product-bound structure, between GmhA-D94 and bound product. Asp-94 is unique among residues mutated within the active site and is of particular interest because it is donated from the opposing dimer (chain B). Other residues contributing to substrate or product binding originate from the A–D dimer. Sedimentation equilibrium analysis of both the wild-type GmhA and GmhA-D94N mutant indicate that the *E. coli* protein exists as a tetramer in solution. Structural and mutational data also support a tetrameric GmhA, because the *E. coli* protein crystallized as a tetramer in the asymmetric unit and mutation of Asp-94 shows at least partial inhibition of GmhA activity. Interestingly, Thr-120 (conserved phosphate binding pocket) and Asp-94 (H3′ region) belong to regions of GmhA primarily involved in product binding. Results from mutational studies are therefore consistent with the possibility that product stabilization is an important mechanism used by GmhA to establish desired isomerization reaction kinetics.

Given that Glu-65 and His-180 were identified as the most critical residues for GmhA activity, a mechanism of action of GmhA can be proposed by analogy to other known aldo-keto isomerases, with Glu-65 and His-180 acting as the catalytic residues. Histidine residues are often found involved in isomerase activity, acting most frequently as a catalytic base, facilitating the reaction through proton shuffling (41, 42). Specifically, the active site of the isomerase domain of glucosamine 6-phosphate (Gln6P) synthase has been shown to rely on His and Glu residues (43, 44). This enzyme shares the greatest structural similarity to GmhA among currently characterized isomerases (25). A structural comparison of the quaternary and active site structures of these two isomerase enzymes is provided in supplemental Fig. S4. As expected, a collection of four serine and threonine residues forms a structurally conserved phosphate-binding pocket. The catalytic Glu-65 residue identified in *E. coli* GmhA is also structurally conserved. Further similarity exists for His-180, which is replaced by a lysine (Lys-485) in Gln6P synthase, where the catalytic lysine (Lys-603) of Gln6P synthase has no homologous residue in GmhA. The catalytic histidine (His-504) of Gln6P is not conserved structurally; however, it does reside close to Asp-94 within GmhA. Unlike Gln6P synthase, though, mutational analysis does not suggest that GmhA requires a third residue for activity, as fulfilled by His-504 in Gln6P synthase, suggesting the S7P sugar ring opens non-enzymatically prior to catalysis. Interestingly, although Gln6P synthase exists as a dimer, each monomer contains two structurally

related domains (supplemental Fig. S4*A*). Each of these domains is homologous to a single monomer of GmhA. Thus, similar to GmhA, the isomerase portion of Gln6P synthase adopts an overall quaternary structure comprised of four structurally equivalent domains. This finding provides additional support for the biological significance of a GmhA tetramer.

A potential mechanism of action for GmhA, based on previous studies of the isomerase domain from Gln6P synthase, is outlined in Fig. 8. This mechanism proposes that either Glu-65 or His-180 could act as the catalytic base, abstracting a proton from C2 of the S7P substrate, while the other residue would act as a catalytic acid, donating a proton to C1 for stabilization. The reaction then proceeds through the resulting *cis*-enediol intermediate resulting in an aldo form, which then cycles non-enzymatically to give the final product, D-*glycero*-α,β-D-*manno*-heptose 7-phosphate. Although it is difficult to predict which residue, Glu-65 or His-180, performs each catalytic role, based on the complete absence of any activity when Glu-65 is mutated, it can be hypothesized that Glu-65 assumes the critical role of the catalytic base in this mechanism.

Together the crystallographic and mutational studies presented here offer new insight into the structure-function relationship of GmhA, an essential protein in maintaining the permeability barrier of Gram-negative bacteria. GmhA is highly conserved between pathogenic species, both in sequence and structure. As such, knowledge gained from the current studies of GmhA from *E. coli* and *P. aeruginosa* should be readily transferable to other pathogenic Gram-negative species. Inhibition of GmhA, in synergy with known Gram-positive antimicrobial agents, may aid in treatment of Gram-negative infection. An understanding of the structure and mechanism of GmhA are the first steps in exploiting the heptose biosynthetic pathway as a novel Gram-negative antimicrobial target.

Acknowledgments—We thank Kalinka Koteva and Don Hughes for assistance with substrate synthesis and J. Osipuik of the Midwest Center for Structural Genomics for collecting the selenomethionine P. aeruginosa diffraction data.

REFERENCES

1. Raetz, C. R., and Whitfield, C. (2002) *Annu. Rev. Biochem.* **71,** 635–700
2. Nikaido, H. (2003) *Microbiol. Mol. Biol. Rev.* **67,** 593–656
3. Nikaido, H., and Vaara, M. (1985) *Microbiol. Rev.* **49,** 1–32
4. Yethon, J. A., and Whitfield, C. (2001) *Curr. Drug Targets Infect. Disord.* **1,** 91–106
5. Onishi, H. R., Pelak, B. A., Gerckens, L. S., Silver, L. L., Kahan, F. M., Chen, M. H., Patchett, A. A., Galloway, S. M., Hyland, S. A., Anderson, M. S., and Raetz, C. R. (1996) *Science* **274,** 980–982
6. Valvano, M. A., Messner, P., and Kosma, P. (2002) *Microbiology* **148,** 1979–1989
7. Wright, G. D., and Sutherland, A. D. (2007) *Trends Mol. Med.* **13,** 260–267
8. Kneidinger, B., Marolda, C., Graninger, M., Zamyatina, A., McArthur, F., Kosma, P., Valvano, M. A., and Messner, P. (2002) *J. Bacteriol.* **184,** 363–369
9. Eidels, L., and Osborn, M. J. (1971) *Proc. Natl. Acad. Sci. U. S. A.* **68,** 1673–1677
10. Kneidinger, B., Graninger, M., Puchberger, M., Kosma, P., and Messner, P. (2001) *J. Biol. Chem.* **276,** 20935–20944
11. Brooke, J. S., and Valvano, M. A. (1996) *J. Bacteriol.* **178,** 3339–3341
12. Brooke, J. S., and Valvano, M. A. (1996) *J. Biol. Chem.* **271,** 3608–3614
13. Eidels, L., and Osborn, M. J. (1974) *J. Biol. Chem.* **249,** 5642–5648
14. McArthur, F., Andersson, C. E., Loutet, S., Mowbray, S. L., and Valvano, M. A. (2005) *J. Bacteriol.* **187,** 5292–5300
15. Loutet, S. A., Flannagan, R. S., Kooi, C., Sokol, P. A., and Valvano, M. A. (2006) *J. Bacteriol.* **188,** 2073–2080
16. Valvano, M. A., Marolda, C. L., Bittner, M., Glaskin-Clay, M., Simon, T. L., and Klena, J. D. (2000) *J. Bacteriol.* **182,** 488–497
17. Sirisena, D. M., MacLachlan, P. R., Liu, S. L., Hessel, A., and Sanderson, K. E. (1994) *J. Bacteriol.* **176,** 2379–2385
18. Morrison, J. P., and Tanner, M. E. (2007) *Biochemistry* **46,** 3916–3924
19. De Leon, G. P., Elowe, N. H., Koteva, K. P., Valvano, M. A., and Wright, G. D. (2006) *Chem. Biol.* **13,** 437–441
20. Grossman, T. H., Kawasaki, E. S., Punreddy, S. R., and Osburne, M. S. (1998) *Gene* (*Amst.*) **209,** 95–103
21. Qoronfleh, M. W., Ho, T. F., Brake, P. G., Banks, T. M., Pulvino, T. A., Wahl, R. C., Eshraghi, J., Chowdhury, S. K., Ciccarelli, R. B., and Jones, B. N. (1995) *J. Biotechnol.* **39,** 119–128
22. O'Gara, M., Adams, G. M., Gong, W., Kobayashi, R., Blumenthal, R. M., and Cheng, X. (1997) *Eur. J. Biochem.* **247,** 1009–1018
23. Pflugrath, J. W. (1999) *Acta Crystallogr. D Biol. Crystallogr.* **55,** 1718–1725
24. Vagin, A., and Teplyakov, A. (1997) *J. Appl. Crystallogr.* **30,** 1022–1025
25. Seetharaman, J., Rajashankar, K. R., Solorzano, V., Kniewel, R., Lima, C. D., Bonanno, J. B., Burley, S. K., and Swaminathan, S. (2006) *Proteins* **63,** 1092–1096
26. Otwinoski, Z., and Minor, W. (1997) *Methods Enzymol.* **276,** 307–326
27. Terwilliger, T. C., and Berendzen, J. (1999) *Acta Crystallogr. D Biol. Crystallogr.* **55,** 849–861
28. Terwilliger, T. C. (2000) *Acta Crystallogr. D Biol. Crystallogr.* **56,** 965–972
29. Jones, T. A., Zou, J. Y., Cowan, S. W., and Kjeldgaard, M. (1991) *Acta Crystallogr. A* **47 (Pt 2),** 110–119
30. Emsley, P., and Cowtan, K. (2004) *Acta Crystallogr. D Biol. Crystallogr.* **60,** 2126–2132
31. Murshudov, G., Vagin, A., and Dodson, E. (1996) in *Abstr. Proc. Daresbury Study Weekend*, pp. 93–104, SERC, Daresbury Laboratory, Warrington, UK
32. Brunger, A. T., Adams, P. D., Clore, G. M., DeLano, W. L., Gros, P., Grosse-Kunstleve, R. W., Jiang, J. S., Kuszewski, J., Nilges, M., Pannu, N. S., Read, R. J., Rice, L. M., Simonson, T., and Warren, G. L. (1998) *Acta Crystallogr. D Biol. Crystallogr.* **54,** 905–921
33. Fraternali, F., and Cavallo, L. (2002) *Nucleic Acids Res.* **30,** 2950–2960
34. Lee, S., Kirschning, A., Muller, M., Way, C., and Floss, H. G. (1999) *J. Mol. Catal. B Enzym.* **6,** 369–377
35. Fukui, K., Momoi, K., Watanabe, F., and Miyake, Y. (1988) *Biochemistry* **27,** 6693–6697
36. Baba, T., Ara, T., Hasegawa, M., Takai, Y., Okumura, Y., Baba, M., Datsenko, K. A., Tomita, M., Wanner, B. L., and Mori, H. (2006) *Mol. Syst. Biol.* **2,** 2006–2008
37. Marolda, C. L., Lahiry, P., Vines, E., Saldias, S., and Valvano, M. A. (2006) *Methods Mol. Biol.* **347,** 237–252
38. Tsai, C. M., and Frasch, C. E. (1982) *Anal. Biochem.* **119,** 115–119
39. Krissinel, E., and Henrick, K. (2007) *J. Mol. Biol.* **372,** 774–797
40. Tamaki, S., Sato, T., and Matsuhashi, M. (1971) *J. Bacteriol.* **105,** 968–975
41. Berrisford, J. M., Hounslow, A. M., Akerboom, J., Hagen, W. R., Brouns, S. J., van der Oost, J., Murray, I. A., Michael Blackburn, G., Waltho, J. P., Rice, D. W., and Baker, P. J. (2006) *J. Mol. Biol.* **358,** 1353–1366
42. Knowles, J. R. (1991) *Nature* **350,** 121–124
43. Milewski, S., Janiak, A., and Wojciechowski, M. (2006) *Arch. Biochem. Biophys.* **450,** 39–49
44. Teplyakov, A., Obmolova, G., Badet-Denisot, M.-A., Badet, M., and Polikarpov, B. I. (1998) *Structure* **6,** 1047–1055